Short-range order in Cu-Pt alloys

1993 J. Phys.: Condens. Matter 5 4099

(http://iopscience.iop.org/0953-8984/5/24/011)

J. Phys.: Condens. Matter 5 (1993) 4099–4110. Printed in the UK

Short-range order in Cu–Pt alloys

Dilip Kumar Saha and Ken-ichi Ohshima
Institute of Applied Physics, University of Tsukuba, Tsukuba 305, Japan

Received 15 January 1993

Abstract. The x-ray diffuse scattering intensity from disordered Cu–Pt alloys whose compositions were Cu–7.0, 10.0, 16.0, 24.5, 32.0 and 75.0 at.% Pt was measured at room temperature. Twofold and fourfold splittings of diffuse scattering due to short-range order (SRO) were observed at 100, 110 and their equivalent positions (X points), respectively, for Cu–16.0, 24.5 and 32.0 at.% Pt alloys, where the separation of split diffuse maxima increases monotonically with increasing Pt content. On the other hand, no splitting of diffuse scattering was observed at Cu–< 16.0 at.% Pt alloys. Extra diffuse maxima were observed at $\frac{1}{2}\frac{1}{2}\frac{1}{2}$ and its equivalent positions (R points) for all samples, the intensity being related to the concentration. The SRO parameters were determined from all six alloys. The sign and magnitude of α_{200} strongly depend on the ratio of R- to X-point diffuse intensities. Synthesized data indicated that the first few SRO parameters dominate the R-point maxima, though the sign and magnitude of higher-order parameters play an important role in causing the appearance of split diffuse maxima. It is proposed that there are two types of correlation in the disordered state of the Cu–Pt alloy system, i.e. between the consecutive (111) atomic layers and due to Fermi surface imaging.

1. Introduction

Measurement of the short-range order (SRO) diffuse scattering intensity from materials in order to aid the understanding of structural fluctuations is important. In the Cu–Pt alloy system, the existence of three kinds of ordered phase, Cu_3Pt, CuPt and $CuPt_3$, has been established. In the Cu_3Pt phase region, the $L1_2$- and $L1_{2-S}$-type structures appear below the composition-dependent transition temperature T_c. The CuPt phase has a rhombohedral superstructure of the $L1_1$ type consisting of alternating (111) planes of Cu and Pt atoms (Johansson and Linde 1927, Schneider and Esch 1944). In the $CuPt_3$ phase region, the existence of the three different superlattice structures (rhombohedral, orthorhombic and cubic) has been established, each of which depends on composition and temperature (Miida and Watanabe 1974). Above the transition temperature, this alloy system shows the face-centred cubic structure over the whole composition range.

X-ray studies of the SRO in the Cu–Pt alloys, CuPt (Walker 1952) and alloys with compositions ranging from 4 to 43 at.% Pt (Kaplow 1958), have been made and the SRO parameters determined. However, the detailed distribution of the diffuse scattering intensities in reciprocal space was not given, because powder samples were used in the studies. The SRO diffuse scattering from disordered Cu–Pt alloys with compositions ranging from 24 to 76 at.% Pt were studied by electron diffraction (Ohshima and Watanabe 1973). Twofold and fourfold splittings of diffuse scattering were observed at 100, 110 and their equivalent positions in the composition ranges up to about 45 at.% in their study. The result was interpreted in terms of the Fermi surface imaging theory proposed by Krivoglaz (1969). They also observed the diffuse maxima at $\frac{1}{2}\frac{1}{2}\frac{1}{2}$ and its equivalent positions in

0953-8984/93/244099+12$07.50

addition to the split diffuse maxima. Chevalier and Stobbs (1979) have reported that the SRO in quenched CuPt can be approximately classed as microdomain in nature. This was determined by electron diffraction and microscopy. Recently, Banhart *et al* (1989) have investigated the effects of SRO on the electronic structure of the Cu–Pt alloy system using the fully relativistic Korringa–Kohn–Rostoker embedded-cluster method (KKR–ECM). The results show the density of states behaviour at the Fermi energy with respect to the SRO parameters for the first- and second-nearest neighbours. A theoretical study of the pressure-induced phase transition for CuPt alloy has also been carried out by Takizawa *et al* (1991). They calculated the rhombohedral distortion of the $L1_1$ structure along the $\langle 111 \rangle$ direction with a maximum value of 1.98° and pointed out that it is not possible to realize the B_2-type structure in the CuPt alloy even at high pressure due to high relativistic effect.

It is therefore of great interest to obtain a series of composition-dependent SRO diffuse intensities and SRO parameters by using x-ray diffuse scattering techniques for the disordered Cu–Pt alloys to understand local atomic arrangements. In particular, there have been no reports on the shape of diffuse scattering from < 24 at.% Pt alloys, even by electron diffraction studies, and there have been no reports on SRO diffuse intensities from single-crystal Cu–Pt alloys using the x-ray method. In this study we have measured the x-ray diffuse intensities from six disordered Cu–Pt alloys. SRO parameters were determined after analysing the composition-dependent diffuse intensities. Local atomic arrangements of Pt atoms were constructed by computer simulation.

2. Experimental procedure

Alloys with compositions less than 20 at.% Pt were prepared in evacuated silica tubes by melting 99.99% pure Cu and Pt, and those with compositions higher than 20 at.% Pt were prepared in high-purity alumina crucibles and melted several times to homogenize. Finally, single crystals were grown by the Bridgman technique. Sample slices of different dimensions from $10 \times 8 \times 3$ mm^3 to $15 \times 9 \times 3$ mm^3 were cut parallel to a (210) plane from their original ingots. The slices were polished mechanically and etched chemically and electrically to remove the distorted surface layer. For Cu–24.5, 32.0 and 75.0 at.% Pt alloys, chemical etching was performed using 30% HNO_3, 10% HCl, 10% H_3PO_4 and 50% CH_3COOH solution at 75 °C in a hot water bath. For Cu–7.0, 10.0 and 16.0 at.% Pt alloys, electrical etching was performed by using 50% H_3PO_4 and 50% H_2O solution using a copper bar as a cathode. All the specimens were annealed separately in evacuated silica tubes at 1050 °C for four days, 1000 °C for one day and 900 °C for ten days successively to homogenize the specimens and were finally quenched by being dropped into iced water. The surface of the specimens was etched again to remove the oxide layer.

Lattice parameters of the specimens, which were prepared separately, were measured with an x-ray Debye–Scherrer camera using Cu Kα radiation. Specimen compositions were determined with an accuracy of ± 0.3 at.% by means of the lattice parameter (a_0)–composition relation (Pearson 1958). The six compositions were determined as Cu–7.0, 10.0, 16.0, 24.5, 32.0 and 75.0 at.% Pt, respectively.

The x-ray intensity measurements were performed at room temperature by using a four-circle goniometer attached to the rota unit of an x-ray generator (Rigaku, RU-300). The incident beam, Cu Kα radiation, from a Cu target was monochromated by a singly bent HOPG crystal. In order to eliminate the $\lambda/2$ harmonics the Ross balanced filter technique was used. This method uses Ni and Co filters with balanced thicknesses placed in front of the scintillation counter alternately. The diffuse intensities were measured by scanning

a volume of reciprocal space at intervals of $\Delta h_i = 1/40$ in terms of the distance between the 000 and 200 fundamental spots. Both background and air scattering were estimated by irradiating an Si single crystal and were subtracted from the measured intensity.

After subtracting both the Bragg intensity near the fundamental spots and the contribution from Compton scattering, the measured intensities were converted to absolute units by comparing them with the intensity scattered from polystyrene (C_8H_8) at $2\theta = 100°$ and integrated intensities from a powdered Al sample. The conversion factors of these two independent methods agreed within ±5%. The intensity distributions due to SRO were separated using the Borie and Sparks (1971) method after removing the size-effect modulation, the Huang scattering and the thermal diffuse scattering from the total diffuse intensities for all the samples.

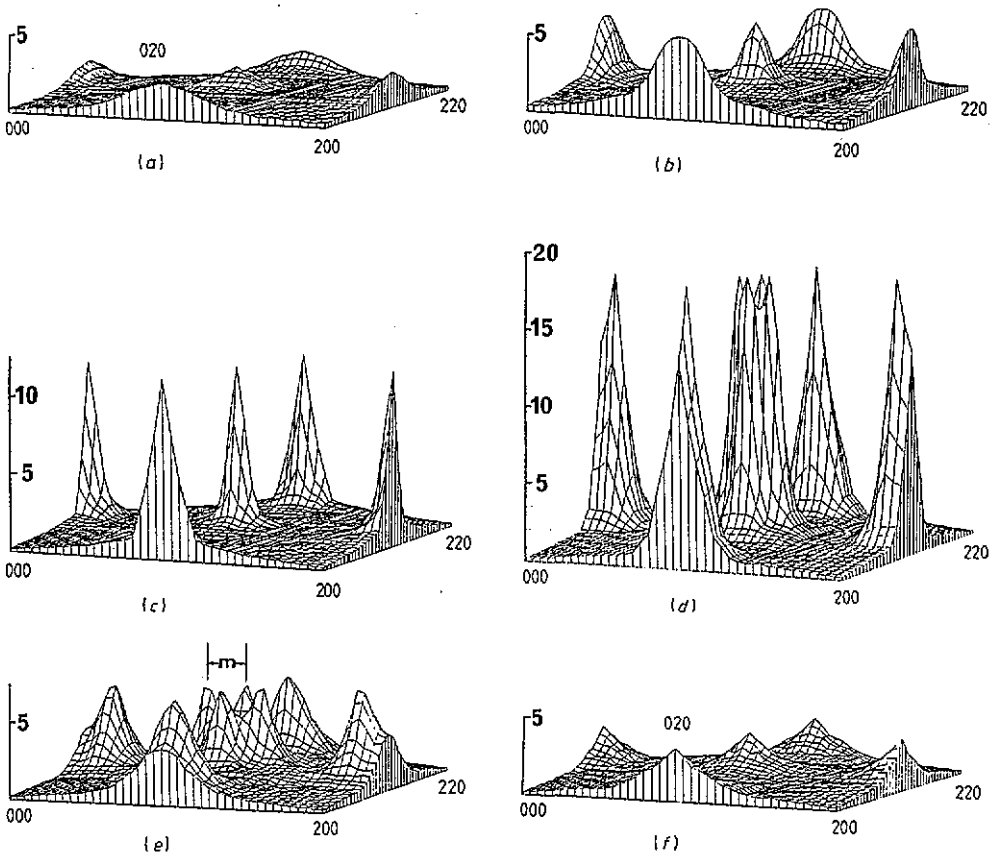

Figure 1. Bird's eye drawings of SRO diffuse scattering intensity distributions on the ($hk0$) reciprocal lattice plane in Laue units for Cu–Pt alloys with (*a*) 7.0, (*b*) 10.0, (*c*) 16.0, (*d*) 24.5, (*e*) 32.0 and (*f*) 75.0 at.% Pt.

3. Results and analysis

The SRO diffuse intensity distributions for all the six alloys are shown on the ($hk0$) reciprocal lattice plane in Laue units in figure 1. As seen in figure 1(*d*) and (*e*), twofold splitting at

the 100 position and fourfold splitting at the 110 position have appeared. The separation between split diffuse maxima at the 110 position related to the distance between the two fundamental spots 000 and 200, which was denoted by m and defined in figure 1(*e*), was measured for the samples and is shown in table 1. The values obtained from an electron-diffraction study (Ohshima and Watanabe 1973) are also given in table 1. The agreement between the two is good. For Cu–16.0 at.% Pt alloy, we found splitting with a very small value of m after carrying out a fine-step scan with $\Delta h_i = 1/200$, though it cannot be seen in figure 1(*c*). On the other hand, no splittings were found in figure 1(*a*), (*b*) and (*f*). In attempting to detect such splitting for dilute cases, we tried the diffuse scattering measurements from Cu–10.0 at.% Pt alloy with the use of a four-circle diffractometer at the BL-4C in the Photon Factory, National Laboratory for High Energy Physics, Tsukuba, Japan using synchrotron radiation. We did not detect any splitting for the sample. From 16.0 to 32.0 at.% Pt alloys, we found that the value of m shows a monotonic increase with increasing Pt content. The intensity distribution for Cu–75.0 at.% Pt alloy is different from that for copper-rich alloys: no splitting of diffuse maxima is seen at 100, 110 and their equivalent positions.

Table 1. Values of separation m measured in terms of the distance between 000 and 200 spots and those from an electron diffraction (Ohshima and Watanabe 1973) study.

at.% Pt	m measured	m obtained from electron diffraction study
7.0	0	—
10.0	0	—
16.0	0.007 ± 0.005	—
24.5	0.080 ± 0.005	0.085 ± 0.005
32.0	0.131 ± 0.005	0.130 ± 0.005
75.0	0	—

The diffuse intensity distributions on the (*hhl*) reciprocal lattice plane in Laue units are shown in figure 2 for all six alloys. Diffuse intensities are obtained at $\frac{1}{2}\frac{1}{2}\frac{1}{2}$ (R point) and its equivalent positions for all the samples in addition to the diffuse maxima at/around 110, 001 and their equivalent positions. In figure 2 it can be seen that with the increase of Pt content the R-point diffuse maxima get sharper. We calculated the full width at half maximum (FWHM) for all diffuse peaks. In figure 3 we plotted both the peak intensities in Laue units and the values of the FWHM in terms of the distance between 000 and 100 spots (a_0^* unit). The value of the FWHM for the R-point diffuse peak increases and its intensity decreases with decreasing Pt content. On the other hand, the FWHM for the diffuse peak at/around the 110 position decreases monotonically with decreasing Pt content. In Cu–32.0 and 75.0 at.% Pt alloys, R-point diffuse maxima are much higher than that from Cu–24.5 at.% Pt alloy. This may be due to the effect of the $L1_1$-type rhombohedral structure in the ordered CuPt phase. On the other hand, in Cu–32.0 and 75.0 at.% Pt alloys, X-point (at/around 100 or 110 point) diffuse maxima are much lower than that from the Cu–24.5 at.% Pt alloy. This may be due to the effect of different ordered structures in the low-temperature phase.

By Fourier inversion of the SRO diffuse scattering intensities, Warren–Cowley SRO parameters α_{lmn} were determined up to the 50th shell for all six disordered Cu–Pt alloys, with an error estimated to be less than ±5%. These values are listed in table 2, where l, m and n are integers. The values of α_{000} are very close to unity for all the data. To

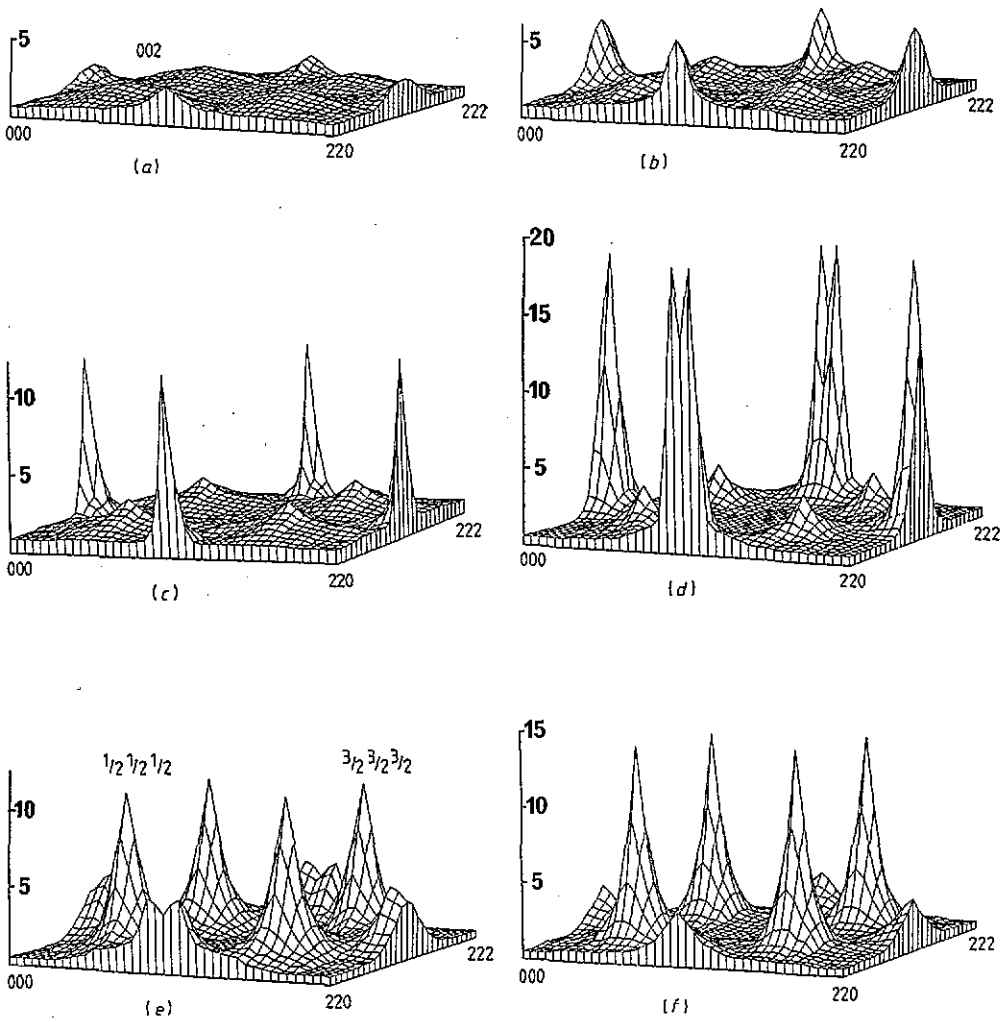

Figure 2. Bird's eye drawing of SRO diffuse scattering intensity distributions on the (*hhl*) reciprocal lattice plane in Laue units for Cu–Pt alloys with (*a*) 7.0, (*b*) 10.0, (*c*) 16.0, (*d*) 24.5, (*e*) 32.0 and (*f*) 75.0 at.% Pt.

understand the characteristics of sign and magnitude of the SRO parameters clearly, we try to determine the partial SRO parameters for Cu–16.0 at.% Pt alloy, α_i^X and α_i^R, for X-point and R-point diffuse intensities, respectively. The first eight values are listed in table 3. α_{200} is characteristically negative (−0.095) for R-point diffuse intensity and positive (0.065) for X-point diffuse intensity. On the other hand, α_{220} and α_{400} are positive and α_{110} is negative for both cases. Total SRO parameters ($\alpha_i^X+\alpha_i^R$) are negative for 110, 200, 211 and 321 shells and positive for 220, 310, 222 and 400 shells. Compared with the experimentally determined SRO parameters, α_i, for the Cu–16.0 at.% Pt alloy in the fifth column of table 3, the agreement between the two is good. It is, therefore, recognized that the sign and magnitude of the SRO parameters depend on the diffuse intensity ratio between the R and X points. We have explained in the introduction that the CuPt ordered phase has a rhombohedral structure

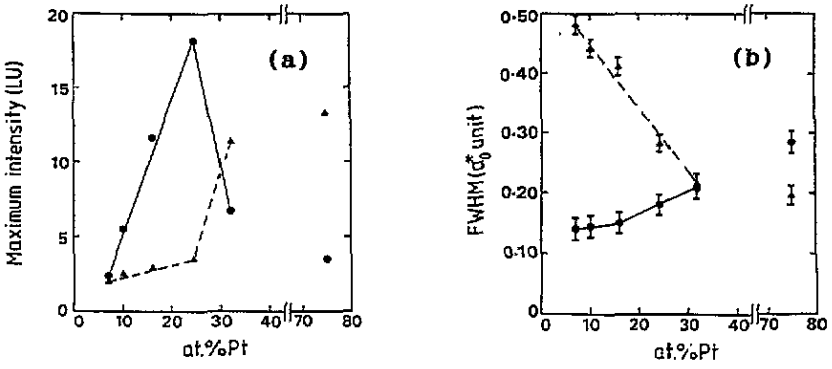

Figure 3. (*a*) Intensity of diffuse maxima in Laue units and (*b*) FWHM in a_0^* units versus at.% Pt: ● at/around the 100 point and ▲ at the $\frac{1}{2}\frac{1}{2}\frac{1}{2}$ point.

consisting of alternating (111) planes of Cu and Pt atoms, where the superlattice reflections are observed at $\frac{1}{2}\frac{1}{2}\frac{1}{2}$ and their equivalent positions in reciprocal space. Long-range order (LRO) parameters for the stoichiometric composition are given as 0, −1, 0, +1, 0 and so on from the first. In the disordered state, the sign of the SRO parameters are of the same order and their magnitudes decrease gradually with increasing interatomic distance. The present values of the Cu–16.0 at.% Pt alloy in table 3, α_i^R, are a little different from those above because of the non-stoichiometric composition.

In table 2, we have seen that the sign of α_{110} is negative for all cases and its absolute values increase with increasing Pt content except for the 75.0 at.% Pt alloy. On the other hand, the sign of α_{200} is negative for all cases except for the Cu–24.5 at.% Pt alloy. From Cu–7.0 to 16.0 at.% Pt alloys, the absolute values of α_{200} decrease with increasing Pt content. In these three cases R-point diffuse intensity increases a little but X-point diffuse intensity increases monotonically with increasing Pt content. In Cu–24.5 at.% Pt alloy, α_{200} is positive (0.075) due to the higher intensity at the X point (18.2) than that at the R point (3.5). Kaplow (1958) has measured the SRO parameters from a powdered sample of Cu–24.0 at.% Pt alloy; a negative α_{110} with a larger magnitude than that of the positive α_{200}, with the largest value of α_{220} being 0.14. In comparison with our data for Cu–24.5 at.% Pt single-crystal alloy, similar trends in parameters were observed. For Cu–32.0 and 75.0 at.% Pt alloys the sign of α_{200} is negative and its absolute value increases with increasing Pt content due to the high-intensity effect at the R point (11.4, 13.3) compared with that at the X point (6.7, 3.5). The sign of α_{220} and α_{400} is positive for all the cases whose absolute values are large and increase monotonically with increasing Pt content. This inclination is understandable in considering the partial SRO parameters described above.

To investigate how the split diffuse maxima for Cu–24.5 and 32.0 at.% Pt alloys are reflected by the SRO parameters the diffuse intensity map was synthesized using a limited number of them. We have noticed that the sign and magnitude of higher-order parameters play an important role in causing the appearance of split diffuse maxima near the 100 and 110 positions, though their absolute values are very small compared with those of the lower-order ones. Only the first few SRO parameters are needed to reconstruct the R-point diffuse scattering for all the samples. We can deduce the so-called correlation length, which is inversely proportional to the FWHM in figure 3(*b*). The correlation length for R-point diffuse maxima increases almost linearly and for X-point diffuse maxima decreases gradually with increasing Pt content except for in the case of the Cu–75.0 at.% Pt alloy.

Table 2. SRO parameters determined from the Fourier transform of the SRO diffuse scattering intensities and one set of those for Cu–24.5 at.% Pt alloy calculated from the model by computer simulation, where N is the shell number.

		at.% Pt						
		7.0	10.0	16.0	24.5		32.0	75.0
N	*lmn*				Expt.	Simul.		
	000	1.004	1.006	1.007	1.010	1.000	1.030	1.005
1	110	−0.054	−0.063	−0.088	−0.108	−0.107	−0.167	−0.053
2	200	−0.052	−0.047	−0.030	0.075	0.075	−0.050	−0.126
3	211	−0.027	−0.016	−0.020	−0.038	−0.038	−0.024	−0.019
4	220	0.017	0.036	0.081	0.124	0.123	0.159	0.133
5	310	0.020	0.019	0.002	−0.005	−0.005	0.012	0.008
6	222	0.012	0.005	0.020	0.056	0.055	−0.013	−0.066
7	321	0.006	0.000	−0.004	−0.019	−0.019	−0.004	0.003
8	400	0.019	0.025	0.046	0.056	0.056	0.059	0.058
9	330	−0.019	−0.012	−0.018	−0.021	−0.021	−0.031	−0.014
	411	0.018	0.004	0.006	−0.029	−0.028	−0.005	0.001
10	420	0.016	0.011	0.017	0.043	0.043	0.005	−0.018
11	332	−0.002	0.000	0.001	−0.009	−0.009	−0.013	−0.004
12	422	0.000	0.005	0.026	0.035	0.034	0.022	0.023
13	431	−0.011	−0.012	−0.006	−0.022	−0.022	−0.015	−0.012
	510	−0.016	−0.011	−0.011	−0.006	−0.006	−0.012	−0.007
14	521	0.001	−0.001	−0.004	−0.004	−0.004	−0.003	−0.004
15	440	−0.012	−0.004	−0.003	0.019	0.019	−0.010	−0.002
16	433	0.003	0.002	0.000	−0.006	−0.006	0.016	0.014
	530	0.011	0.013	0.009	0.009	0.009	0.009	0.009
17	442	−0.002	0.002	0.005	0.020	0.020	0.001	−0.003
	600	−0.039	−0.013	0.007	0.021	0.021	0.000	−0.012
18	532	−0.001	0.000	−0.001	−0.001	−0.001	0.002	0.003
	611	−0.012	−0.011	−0.019	−0.029	−0.028	−0.023	−0.008
19	620	−0.006	−0.001	−0.005	0.016	0.016	0.003	−0.001
20	541	0.000	−0.001	0.001	−0.005	−0.005	0.013	0.006
21	622	−0.002	0.003	0.002	0.019	0.019	0.006	0.002
22	631	0.003	0.001	−0.002	−0.011	−0.011	0.008	0.010
23	444	0.007	0.002	0.005	0.013	0.013	0.004	0.001
24	543	0.001	−0.001	−0.001	−0.006	−0.006	−0.010	−0.010
	550	0.004	−0.001	−0.006	−0.003	−0.003	−0.018	−0.007
	710	0.006	0.004	0.007	0.006	0.006	0.008	0.003
25	640	0.014	0.013	0.011	0.016	0.016	0.013	0.013
26	552	−0.002	0.002	0.001	0.001	0.001	−0.006	0.001
	633	0.000	−0.003	−0.003	−0.014	−0.014	−0.015	−0.016
	721	0.003	0.002	0.002	0.001	0.001	0.003	0.002
27	642	0.001	0.000	0.001	0.008	0.008	−0.007	−0.006
28	730	−0.006	−0.003	−0.003	−0.001	−0.001	−0.006	−0.004
29	651	−0.002	−0.003	−0.003	−0.006	−0.006	0.000	−0.007
	732	−0.002	−0.001	0.000	0.001	0.001	−0.003	−0.001
30	800	0.021	0.014	0.020	0.012	0.011	0.011	0.002
31	554	−0.003	−0.001	0.001	0.000	0.000	0.007	0.008
	741	−0.001	−0.003	−0.001	−0.002	−0.002	0.000	−0.004
	811	0.013	0.006	0.009	−0.013	−0.013	0.004	0.007
32	644	0.001	0.002	0.000	0.008	0.008	−0.003	0.001
	820	0.014	0.008	0.014	0.018	0.018	0.016	0.010
33	653	0.000	0.000	−0.002	−0.002	−0.002	0.011	0.010
34	660	−0.005	−0.005	−0.010	−0.001	−0.001	−0.029	−0.014

Table 2. (continued)

		at.% Pt						
		7.0	10.0	16.0	24.5		32.0	75.0
N	*lmn*				Expt.	Simul.		
	822	−0.001	0.000	0.002	0.007	0.007	−0.004	−0.008
35	743	0.002	0.002	0.001	0.001	0.001	0.008	0.005
	750	0.002	0.005	0.004	0.002	0.002	−0.002	0.005
	831	−0.007	−0.007	−0.006	−0.016	−0.016	−0.015	−0.011
36	662	−0.001	0.001	0.001	0.006	0.006	0.003	0.009
37	752	−0.001	0.001	0.000	0.000	0.000	−0.003	0.001
38	840	−0.013	−0.009	−0.007	0.000	0.000	−0.020	−0.017
39	833	0.003	0.002	0.001	−0.002	−0.002	0.014	0.016
	910	−0.004	−0.001	−0.002	0.002	0.002	−0.002	0.000
40	842	−0.004	0.000	0.003	0.007	0.007	0.006	0.010
41	655	0.000	−0.001	−0.001	−0.004	−0.004	−0.006	−0.007
	761	0.000	0.000	0.000	0.001	0.001	0.010	0.003
	921	0.000	0.000	0.000	0.001	0.001	0.000	0.000
42	664	−0.001	0.001	0.002	0.005	0.005	0.002	−0.002
43	754	0.000	0.000	−0.001	−0.002	−0.002	−0.005	−0.004
	930	0.001	0.002	0.003	0.006	0.006	0.002	0.003
	851	0.002	0.001	0.001	−0.001	−0.001	0.010	0.005
44	763	0.000	−0.001	−0.001	−0.002	−0.002	−0.003	−0.005
	932	0.001	0.001	0.000	0.001	0.001	0.001	0.000
45	844	0.004	0.003	0.003	0.005	0.005	−0.001	−0.003
46	770	0.002	0.002	0.001	0.001	0.001	−0.003	0.005
	853	0.000	−0.001	0.000	−0.005	−0.005	−0.007	−0.011
	941	−0.001	−0.001	0.000	0.001	0.001	0.004	0.001
47	860	0.003	0.003	0.003	0.000	0.000	−0.004	0.001
	1000	0.000	0.000	0.000	0.000	0.000	0.000	0.000
48	772	0.001	0.000	0.001	−0.002	−0.002	−0.003	0.000
	1011	−0.015	−0.011	−0.016	−0.019	−0.019	−0.016	−0.007
49	862	0.000	0.000	0.000	0.000	0.000	−0.013	−0.009
	1020	0.000	−0.001	0.000	−0.001	−0.001	−0.006	−0.006
50	943	0.000	0.000	0.000	−0.001	−0.001	0.000	−0.001
	950	0.000	0.000	0.000	0.000	0.000	0.000	0.000

Table 3. Partial SRO parameters α_i^X and α_i^R for X-point and R-point diffuse intensities, respectively, and experimentally determined SRO parameters α_i for the Cu–16.0 at.% Pt alloy.

lmn	α_i^X	α_i^R	$(\alpha_i^X + \alpha_i^R)$	α_i
110	−0.053	−0.040	−0.093	−0.088
200	0.065	−0.095	−0.030	−0.030
211	−0.007	−0.014	−0.021	−0.020
220	0.058	0.027	0.085	0.081
310	−0.020	0.026	0.006	0.002
222	0.030	−0.006	0.024	0.020
321	−0.010	0.000	−0.010	−0.004
400	0.024	0.022	0.046	0.046

The correlation length for the Cu–32.0 at.% Pt alloy in both cases is about $5a_0$.

4. Local structure

A possible local atomic arrangement could be constructed by using the observed SRO parameters and a simulation program (Suzuki *et al* 1982, Ohshima *et al* 1987, Saha *et al* 1992). More than 40th shell SRO parameters were adjusted so as to fit the experimentally determined α_{lmn} values for the atomic arrangements of $10 \times 10 \times 10$ FCC unit cells. Two sets of results for Cu–16.0 and 24.5 at.% Pt alloys are shown in figure 4(*a*) and (*c*) for the ideally random arrangement (RANDOM) in which all the SRO parameters are fitted to zero except for $\alpha_{000} = 1$ and (*b*) and (*d*) for the observed SRO structures. The computer simulated SRO parameters were compared with those determined by experiment and one set of these parameters is shown in table 2: the agreement between them can be seen. It has been confirmed that the results are fairly good. Similar results were found for other Cu–Pt alloys in this study.

It is difficult to identify structural differences between the RANDOM and SRO states of figure 4(*a*) and (*b*) for the Cu–16.0 at.% Pt alloy because the numbers of Pt–Pt atom pairs of second-nearest neighbours in both cases are almost equal (313 and 275 for RANDOM and SRO, respectively). On the other hand, in figure 4(*c*) and (*d*) for the Cu–24.5 at.% Pt alloy, it is easy to see the difference between the RANDOM and SRO structures because the numbers of Pt–Pt atom pairs of second-nearest neighbours are higher in the SRO state and the numbers of first-nearest neighbours are higher in RANDOM. In figure 4(*a*) and (*c*) some equilateral triangles are seen which are connected by first-nearest neighbours and the numbers increase with increasing Pt content. In figure 4(*c*), four equilateral triangles are joined together and form a large equilateral triangle at the top right corner of the front face. We expect such large equilateral triangles in alternate (111) atomic planes in SRO states. Though there are some equilateral triangles in figure 4(*b*) and (*d*), we do not assume such structural characteristics from the figures directly.

To find the characteristics of the layered structure we separated all the (111) planes from the simulated structures. In figure 5 the Pt atoms on four consecutive (111) planes are represented, where $l + m + n$ are 20, 18, 16 and 14, for the Cu–24.5 at.% Pt alloy (*a*) for a RANDOM and (*b*) for an SRO state. Some Pt atoms are found at the same positions on alternate (111) planes (filled circles) where the interceding alternate (111) planes have Cu atoms (not shown) at the same equivalent positions. On the other hand, open circles indicate Pt atoms on the (111) planes where the interceding alternate (111) planes have no Cu atoms at the same equivalent positions. The number of filled circles in the RANDOM state is very small but in the SRO state this number is around 40% of the total Pt atoms in the plane. This is an example of the layered structure. Due to non-stoichiometric composition, we could not find the above-mentioned Cu and Pt atom symmetry at all equivalent positions.

5. Discussion

We have several reasons for measuring the SRO diffuse intensity from Cu–Pt single-crystal alloys using x-ray diffraction. One is to observe the shape of diffuse intensity in the whole range of Pt content, in particular, from Cu–< 24.0 at.% Pt alloys. Unfortunately, we did not select a sample of Cu–40.0 to 60.0 at.% Pt alloys due to their high T_c. The other reasons are to determine/confirm the existence and origin of R-point diffuse maxima throughout the system. It is peculiar to find this R-point diffuse intensity in the Cu–< 24.5 at.% Pt alloys. We could not expect such R-point diffuse intensity from the Cu_3Pt ordered phase. To find out how R-point diffuse intensity would be changed in the ordered state, three

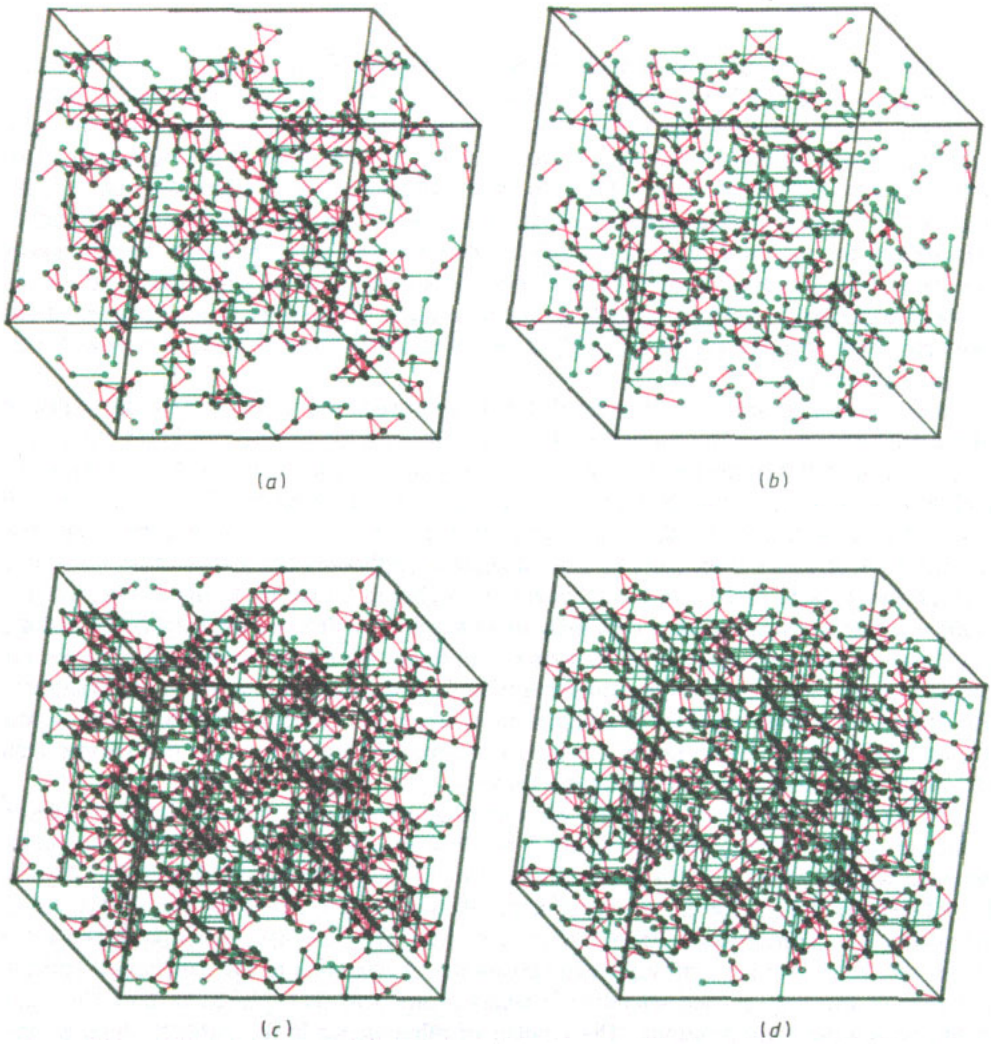

Figure 4. Three-dimensional distributions of Pt atoms simulated on $10 \times 10 \times 10$ FCC unit cells: (*a*) and (*c*) for an ideally RANDOM state and (*b*) and (*d*) for the observed SRO structure for Cu–16.0 and 24.5 at.% Pt alloys, respectively. Only Pt atoms are represented and these are linked together by red and green lines to their first- and second-nearest neighbours, respectively.

samples of Cu–16.0, 32.0 and 75.0 at.% Pt alloys were annealed at 500, 300 and 400 °C, respectively, for 21 days. We have observed an intensity distribution at the R point similar to that obtained for the disordered state of the Cu–16.0 at.% Pt alloy, though superlattice reflections appear at 100, 110 and their equivalent positions due to the Cu_3Pt ordered structure. A much higher and sharper intensity distribution for the Cu–32.0 at.% Pt alloy was observed at the R point, but we did not observe any superlattice reflections at 100, 110 and their equivalent positions. On the other hand, superlattice reflections appear at both the R and X points for Cu–75.0 at.% Pt alloy, due to the existence of the ordered structure (Miida and Watanabe 1974). From these results it is concluded that the short-range correlation between consecutive (111) atomic layers still exists in the Cu_3Pt ordered

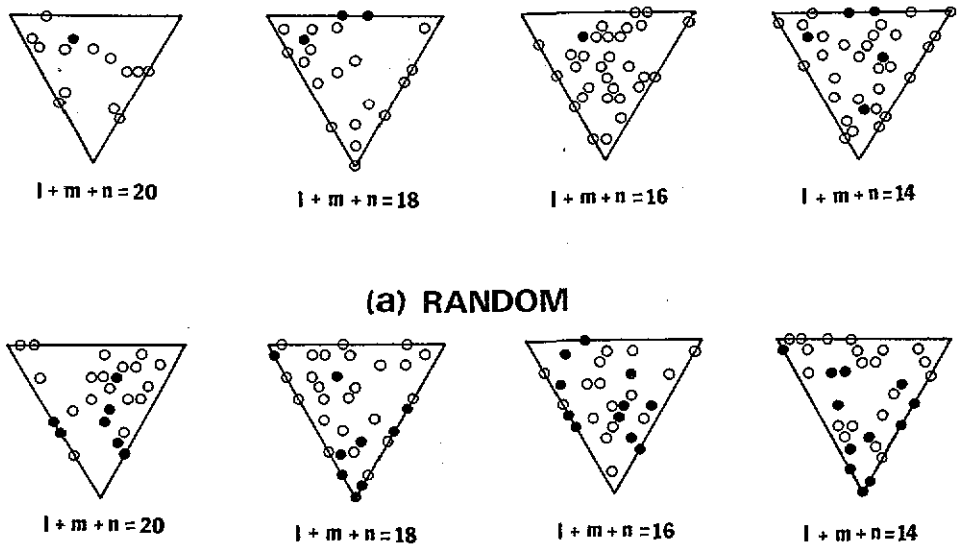

Figure 5. Four consecutive (111) planes where $l + m + n$ are 20, 18, 16 and 14, for the Cu–24.5 at.% Pt alloy separated from figure 4(*c*) and (*d*): (*a*) for a RANDOM state and (*b*) for an SRO state. Filled circles indicate the Pt atoms on the (111) planes where the interceding alternate (111) planes have Cu atoms at the same equivalent positions (not shown). On the other hand, open circles indicate the Pt atoms on the (111) planes where the interceding alternate (111) planes have no Cu atoms at the same equivalent positions.

state and that the correlation develops into ordered structure in the CuPt and $CuPt_3$ regions. It is also concluded that there is no correlation originating from the Fermi surface imaging in the ordered state of the Cu–32.0 at.% Pt alloy though it is present in the disordered state. We, therefore, propose that in the disordered state, there are two types of correlation, i.e. between the consecutive (111) atomic layers and due to Fermi surface imaging. There has been no report of such structural fluctuations in the disordered alloys. This is of interest in calculating the phase stability from the theoretical point of view.

Acknowledgments

The authors would like to express their thanks to Dr Y Watanabe and the staff of the sample preparation room of the Institute for Materials Research, Tohoku University for help in preparing three single-crystal ingots (Cu–24.5, 32.0 and 75.0 at.% Pt alloys), and to Dr K Koga of the University of Tsukuba for his help in analysing the data.

References

Banhart J, Winberger P and Voitlander J 1989 *Phys. Rev.* B **40** 12079
Borie B and Sparks C J 1971 *Acta Crystallogr.* A **27** 198
Chevalier J P and Stobbs W M 1979 *Acta Metall.* **27** 285
Johansson C H and Linde I O 1927 *Ann. Phys.* **82** 449

Kaplow R 1958 *PhD Thesis* MIT (see also Moss S C and Clapp P 1968 *Phys. Rev.* **171** 770)
Krivoglaz M A 1969 *Theory of X-ray and Thermal Neutron Scattering by Real Crystal* (New York: Plenum) p 41
Miida R and Watanabe D 1974 *J. Appl. Crystallogr.* **7** 50
Ohshima K, Iwao N and Harada J 1987 *J. Phys. F: Met. Phys.* **17** 1769
Ohshima K and Watanabe D 1973 *Acta Crystallogr.* A **29** 520
Pearson W B 1958 *A Handbook of Lattice Spacings and Structures of Metals and Alloys* (Oxford: Pergamon) p 597
Saha D K, Koga K and Ohshima K 1992 *J. Phys.: Condens. Matter* **4** 10093
Schneider A and Esch U 1944 *Z. Elektrochem.* **50** 290
Suzuki H, Harada J, Matsui M and Adachi K 1982 *Acta Crystallogr.* A **38** 522
Takizawa S, Blugel S and Terakura K 1991 *Phys. Rev.* B **43** 947
Walker C B 1952 *J. Appl. Phys.* **23** 118